Electronic Supplementary Material (ESI) for Journal of Materials Chemistry C.

Supporting Information

Resistive Switching in Formamidinium Lead Iodide Perovskite Nanocrystals: A Contradiction to the Bulk Form

Chinnadurai Muthu,[a,b] A. N. Resmi,[c] Johnpaul K. Pious,[a,b] G. Dayal,[c] Nayana Krishna,[a] K. B. Jinesh[c] and C .Vijayakumar*[a,b]*

1. Experimental section

Chemicals: Lead iodide (99.999%, Sigma Aldrich), formamidinium iodide (98%, TCI Chemicals), oleylamine (70%, Sigma Aldrich), oleic acid (99%, Alfa Aesar), 1-octadecene (90%, TCI Chemicals) and toluene (99.8%, Merck) were used without further purification.

Measurements: The size and shape of PNCs were studied using FEI-TECNAI T30 high-resolution transmission electron microscopy (HR-TEM), at an accelerating voltage of 300 kV. The TEM samples were prepared by drop-casting toluene suspension of PNCs onto a carbon-coated copper grid at ambient conditions, and the solvent was removed under vacuum. X-ray diffraction study was carried out for film samples with PANalytical X'Pert PRO (Model No. PW 3040/60) using Cu-Kα radiation (λ = 1.5406 Å). The films for XRD analysis were prepared by drop-casting the dispersed PNCs in toluene on the glass plate and dried under vacuum. Electronic absorption spectra were recorded on a Shimadzu UV-2600 UV-vis spectrophotometer, and the emission spectra were recorded on a SPEX-Fluourolog spectrofluorimeter. For colloidal state measurements, the PNCs were dispersed in toluene using sonication. In the case of film, the toluene dispersion was drop cast onto the quartz plate and allowed it to dry under ambient conditions. The oxidation state of the lead metal in PNCs was analyzed using X-ray photoelectron spectroscopy (XPS) using PHI 5000 Versa Probe II having Al kα monochromatic source. The electrical measurements were done using a Cascade four-probe station connected to Agilent B1500A and B2912A parameter analyzers.

Synthesis of α-$FAPbI_3$ nanocrystals: 87 mg of PbI_2 (0.187 mmol) was added into 5 mL of 1-octadecene taken in a 20 mL Schlenk tube and heated to 150 °C for about 15 minutes under vacuum. 0.35 mL of oleylamine and 0.7 mL of oleic acid were injected one by one into the above mixture under nitrogen atmosphere. The mixture was stirred until the complete

solubilization of lead iodide. Subsequently, 80 mg of formamidinium iodide (0.465 mmol) dissolved in 100 μL of DMF and 0.8 mL oleic acid was quickly injected into the lead iodide solution at 80 °C. The resulting perovskite nanocrystals were centrifuged at 12,000 rpm for 5 minutes. The obtained material was washed twice with toluene and dried under vacuum.

2. Size distribution of PNCs

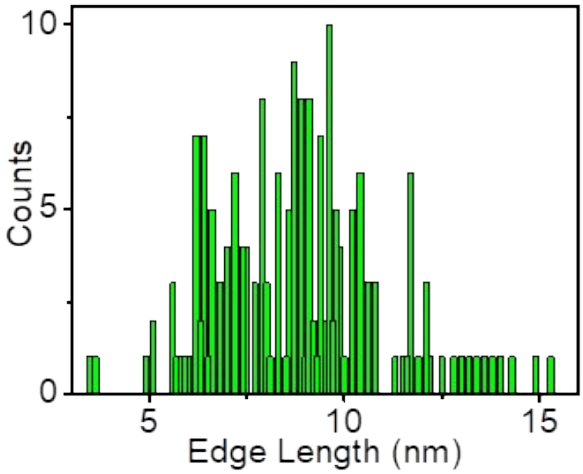

Figure S1. Size distribution profile of PNCs obtained from the TEM image shown in Figure 1a using GATAN Digital Micrograph software (Ver. 2.31.734.0). The average edge length was 9.3 nm.

3. XPS spectra

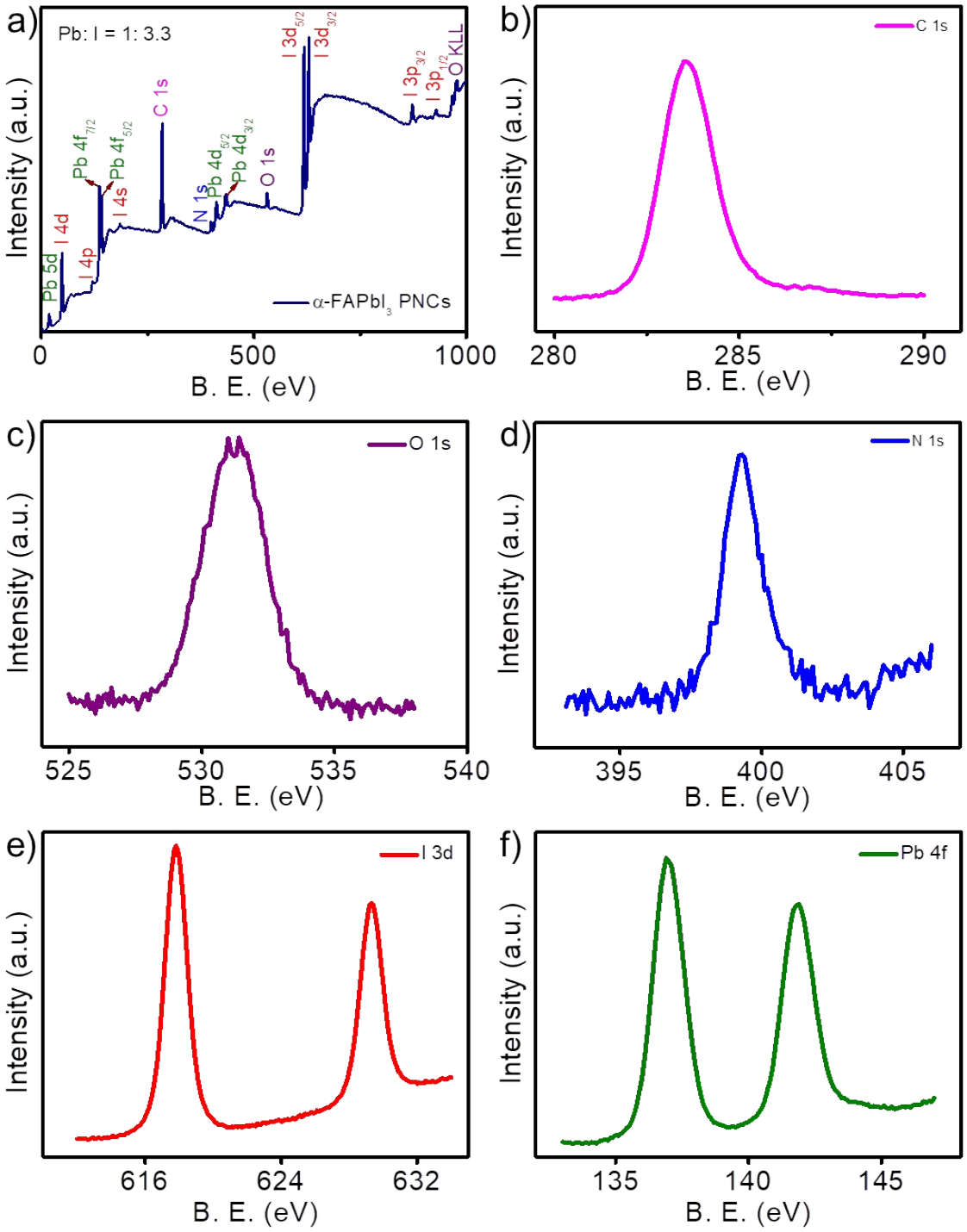

Figure S2. a) XPS survey spectrum of PNCs. XPS profile of PNCs corresponding to b) C 1s, c) O 1s, d) N 1s, e) I 3d, and f) Pb 4f. No additional peaks were observed in all cases confirming the phase purity of the nanocrystals.

4. Morphology analysis

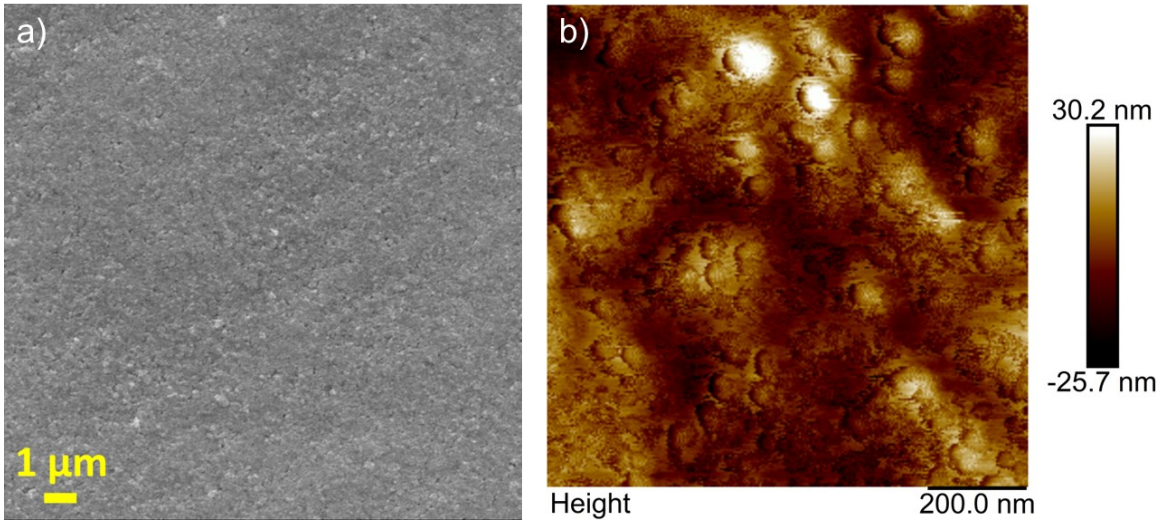

Figure S3. a) SEM and b) AFM images of PNCs film on an FTO substrate. No pin-holes were observed in the samples.

5. Resistive switching

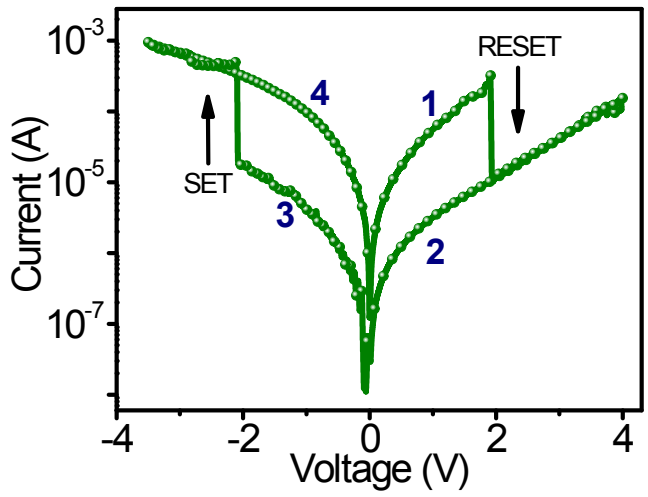

Figure S4. Typical current-voltage (*I-V*) characteristics of a memory device with larger voltage sweeps to check unipolar switching behavior. There is no unipolar switching was observed at higher voltages.

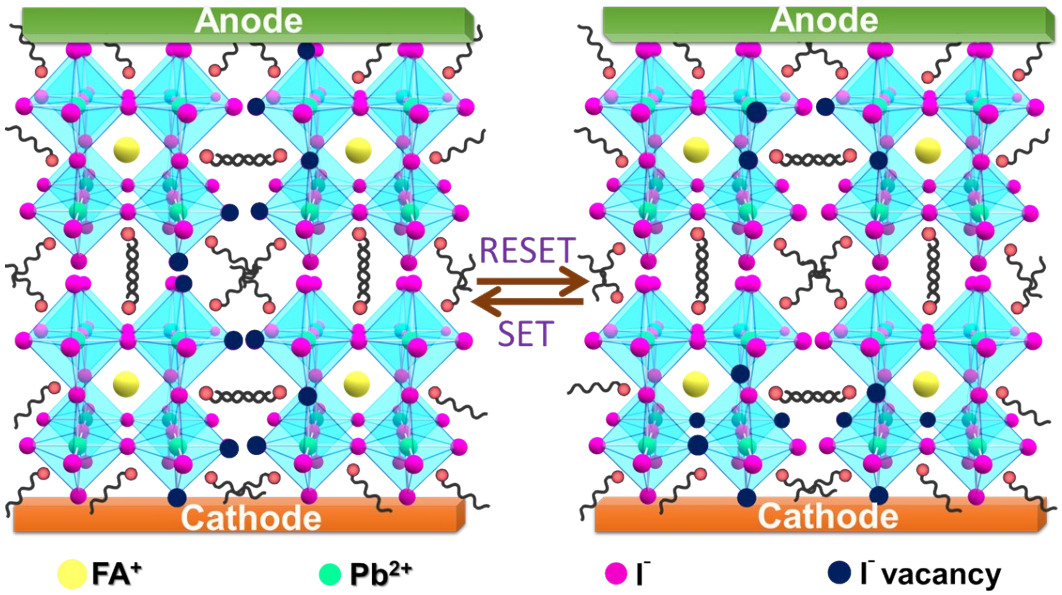

Figure S5. Simplified schematic representation of the 'set' and 'reset' processes in the memory devices.

6. Device-level XPS in-depth analysis

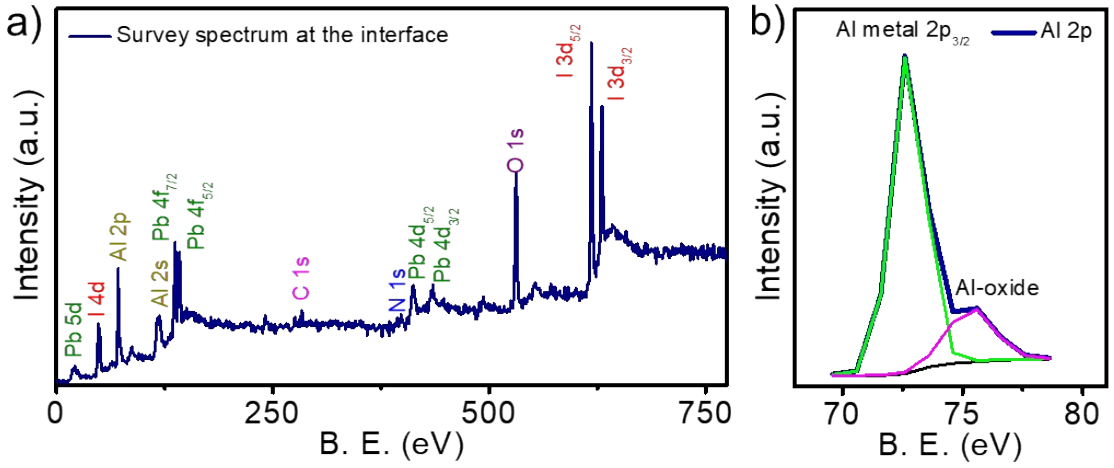

Figure S6. a) In-depth XPS survey spectrum of a PNCs based memory device monitored at the interface between PNC layer and aluminum electrode. b) High resolution XPS profile of Al 2p which shows the presence of AlO_x at the interface.

7. Gold electrode-based memory device

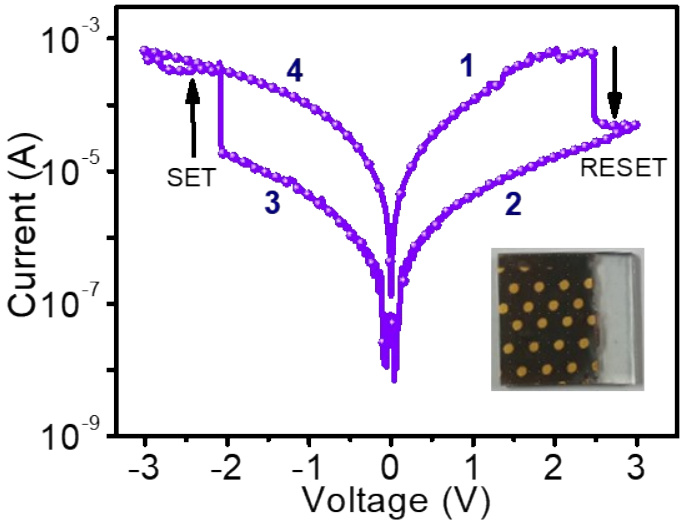

Figure S7. Typical current-voltage (*I-V*) characteristics of a memory device with a structure of FTO/PNCs/Au.

Figure S6 has proved the formation of little aluminum oxide at the PNCs/Al electrode interface during the vapor deposition of Al electrode. To rule out the possibility of the aluminum electrode contribution to resistive switching, memory devices with gold as the top electrode were fabricated and characterized (device structure: FTO/PNCs/Au). The typical current-voltage (*I-V*) characteristics of such a device is shown in **Figure S7**. The device characteristics were similar to that of the aluminum-based devices, confirming that the aluminum electrode has no role in the resistive switching property of PNCs.

8. Stability studies of PNCs

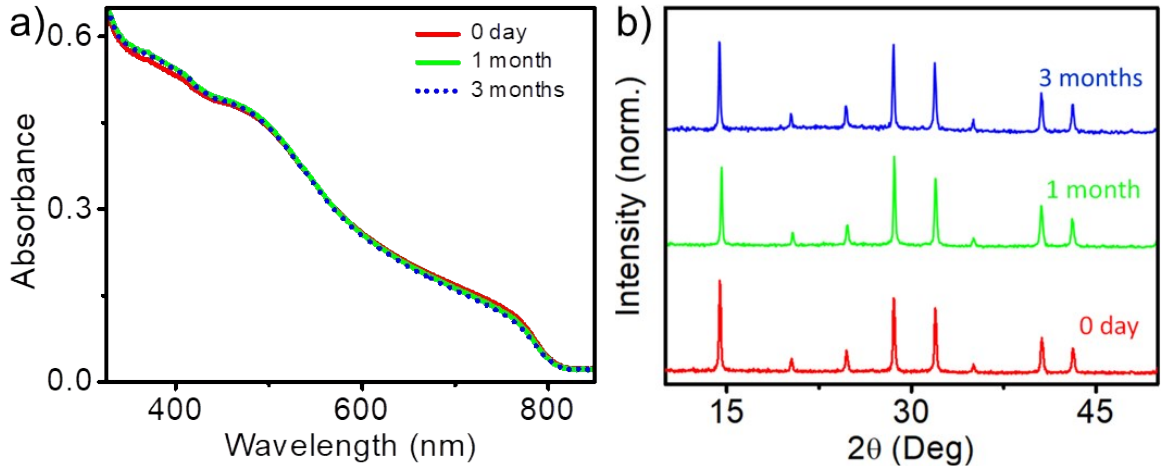

Figure S8. a) Absorption and b) XRD spectra of PNCs taken at different time intervals kept under ambient conditions. The changes were negligible, which indicates excellent phase retention behaviour of the PNCs.

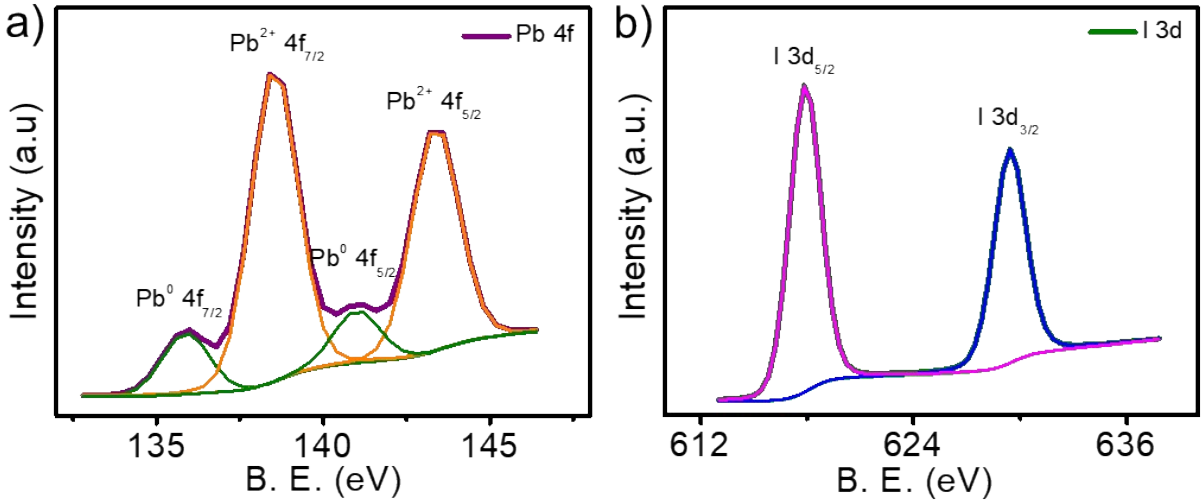

Figure S9. XPS profile of PNCs corresponding to a) Pb 4f and b) I 3d measured in the HRS (off state). Absence of both peak shift and formation of new peaks when compared to that of the LRS state confirmed that no change in crystallinity or phase of the nanocrystals occurs during the switching from LRS to HRS state.

9. Confirmation of Poole-Frenkel conduction

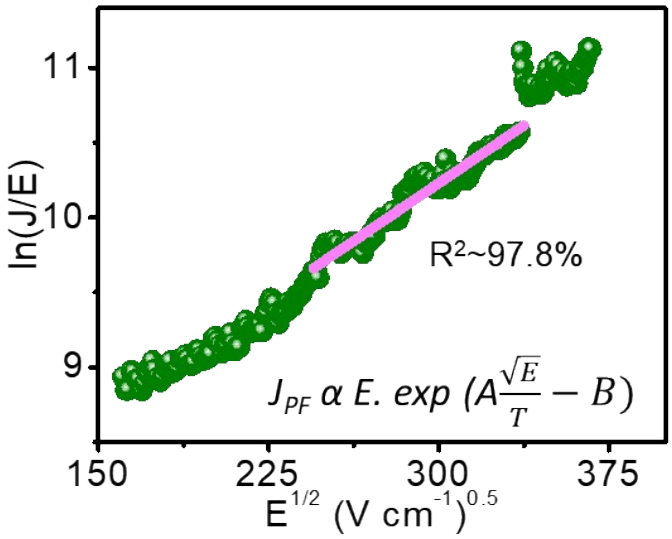

Figure S10. Plot of ln(*J*/*E*) *vs* $E^{1/2}$ of the memory devices in an area within the SCLC region shown in Figure 4a. The proposed mechanism happens in the highlighted regions. A linear relationship between ln(*J*/*E*) and $E^{1/2}$ confirms the Poole-Frenkel conduction mechanism. The R-squared value for the linear fitting is shown in the inset.

10. Endurance data

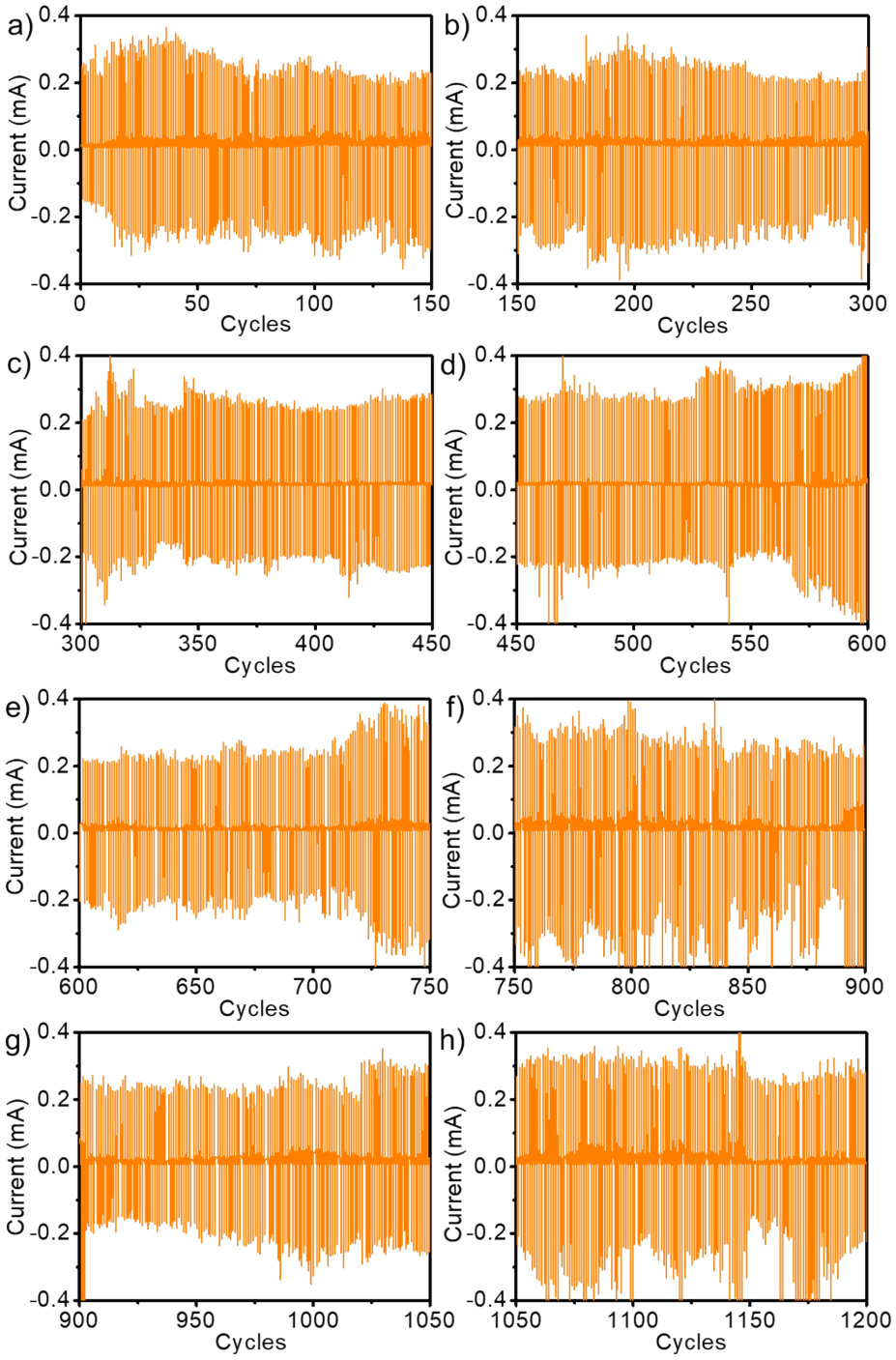

Figure S11. Endurance cycling measurements of the device at pulse voltages of -3, 1, and 3V respectively for 1,200 cycles. The graphs are shown in eight windows for clarity, but the measurement data is continuous.

11. Capping ligand as energy barrier

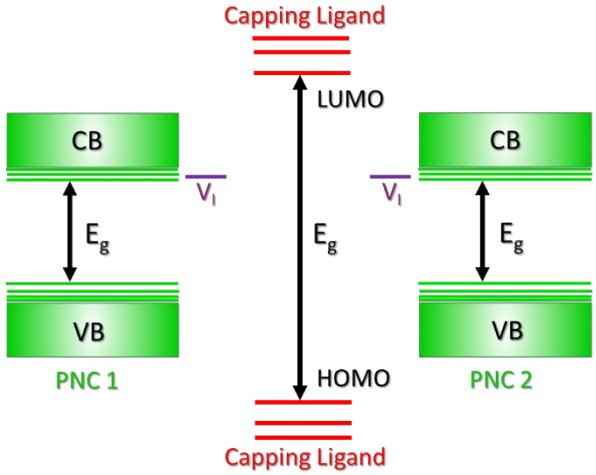

Figure S12. Simplified schematic diagram showing the capping ligands acting as an energy barrier of between two neighbouring PNCs.

12. Resistive switching property comparison table

Table S1. Comparison of the resistive switching properties of α-$FAPbI_3$ PNCs based memory devices (this work) with other PNCs and bulk perovskite devices with a similar device architecture (electrode-perovskite layer-electrode).

S. No	Device structure	Set voltage (V)	Reset voltage (V)	Endurance (cycles)	Retention (time, s)	On/off ratio	Ref.
1	FTO/$CH_3NH_3PbBr_{1.97}Cl_{1.03}$ PNCs/Ag (Our previous work)	+0.7	-0.5	250	1000	10^3	1
2	p^+-Si/Bulk $MAPbI_3$/Al	-3.15	2.21	200	10000	10^3	2
3	FTO/Bulk $MAPbI_3$/Al	-1.2	1.2	100	-	3.5	3
4	FTO/Bulk $MAPbI_3$/Al	+2.5	-1.4	1000	-	20	4
5	ITO/Bulk $MAPbI_3$/Al	+4.7	-1.3	-	-	100	5
6	ITO/Bulk $CsBi_3I_{10}$/Al	-1.7	0.9	150	10000	1000	6
7	FTO/α-$FAPbI_3$ PNCs/Al	-2.4	+2.3	1200	1000	20	This work

The α-$FAPbI_3$ PNCs based devices showed outstanding resistive switching properties compared to bulk perovskites with a comparable device architecture, particularly in terms of endurance and retention properties. Though our device showed low on/off ratio, it could be improved by the incorporation of an insulator layer in the device structure.

13. References

1. C. Muthu, S. Agarwal, A. Vijayan, P. Hazra, K. B. Jinesh, V. C. Nair, *Adv. Mater. Interfaces*, 2016, **3**, 1600092.
2. D. J. Kim, Y. J. Tak, W.-G. Kim, J. K. Kim, J. H. Kim, H. J. Kim, *Adv. Mater. Interfaces,* 2017, **4**, 1601035.
3. Y. Ren, V. Milo, Z. Wang, H. Xu, D. Ielmini, X. Zhao, Y. Liu, *Adv.Theory Simul.,* 2018, **1**, 1700035.
4. Y. Ren, H. Ma, W. Wang, Z. Wang, H. Xu, X. Zhao, W. Liu, J. Ma, Y. Liu, *Adv. Mater., Technol.,* 2019, **4**, 1800238.
5. G. T. S. How, N. A. Talik, B. K. Yap, H. Nakajima, S. Tunmee, B. T. Goh, *Appl. Surf. Sci.,* 2019, **473**, 194.
6. Z. Xiong, W. Hu, Y. She, Q. Lin, L. Hu, X. Tang, K. Sun, *ACS Appl. Mater. Interfaces*, 2019, **11**, 30037.